Turbulent spots in plane Couette flow

John J. Hegseth

Department of Physics, University of New Orleans, Lakefront, New Orleans, Louisiana 70148

An experimental study of the coexistence of laminar flow and turbulent spots in plane Couette flow is presented. Coherent structures within turbulent spots near the critical Reynolds number of this subcritical transition are visualized and studied. Characteristic spanwise lengths and streamwise lengths of the structures are measured. In addition, a characteristic fluctuation time is also measured. These lengths are interpreted as the typical width and typical length of streamwise vortex structures observed to be pervasive in these spots. The characteristic fluctuation time measured the combination of the lifetime and the convective motion of these vortices. The turbulence generating mechanism at the laminar-flow–turbulent-flow interface is discussed. [S1063-651X(96)08010-5]

I. INTRODUCTION

The shear flow driven by the relative motion of two parallel walls at a constant distance apart results in a linear velocity profile. This classic flow, known as plane Couette flow (PCF), is also an exact solution of the governing Navier-Stokes equations. In addition, this simple velocity profile is believed to be linearly stable at all Reynolds numbers R [1]. The Reynolds number is $R = Uh/v$, where U is the speed of the wall, h is half the gap between the walls, and v is the kinematic viscosity. Although a small perturbation cannot destabilize this flow, PCF yields a direct transition to turbulence for finite-amplitude perturbations [2]. The metastability of two distinct states—laminar flow and intermittent turbulence (laminar flow with turbulent spots)—is typical of a transition that can only be generated by finite-amplitude perturbations. Based on an analogy with bifurcation theory this kind of transition is called a subcritical transition [3]. A photograph of the intermittent turbulent state is shown in Fig. 1.

Because of the many practical difficulties involved in PCF, few theoretical, numerical, or experimental results have been obtained. Previous numerical results by Orszag and Kells [4] demonstrated that three-dimensional disturbances can drive the transition to turbulence. The development of turbulent spots was simulated by Lundbladh and Johansson [5]. Three-dimensional (3D) finite-amplitude solutions of PCF were discovered by Nagata [6]. Previous theoretical works by Lerner and Knobloch [7] and Dubrulle and Zahn [8] studied the influence of small velocity profile defects in the inviscid and viscous cases. On the experimental side, Reichardt [9] and Leutheusser [10] observed turbulence in different PCF systems and at different Reynolds numbers. More recently, Tillmark and Alfredsson have studied turbulent spots initiated by localized perturbations [11]. Daviaud [2] reported a detailed study of the transition to turbulence in PCF. They observed the divergence of the average survival time of the spots initiated by localized perturbations and critical fluctuations in this survival time. This behavior is also seen in the critical phenomena of phase transitions. In addition, they also observed traveling waves moving away from the turbulent regions. More recently, Dauchot and Da-

viaud [12] have studied the amplitude dependence of perturbations on the critical Reynolds number, observing a power law. This result explains why so many different and inconsistent observations of the critical Reynolds number have been reported. They have also observed streamwise vortices when the PCF is modified by placing a small wire in the center of the channel along the spanwise direction [13].

II. SYSTEM AND APPARATUS

Various geometries and driving methods have been tried in attempts to make plane Couette flow [9–16]. In our system, vertical walls move in opposite horizontal directions with the same speed resulting in no mean flow [16], as shown in Fig. 2. This has the advantage of simplifying the apparatus while increasing the time available to observe tur-
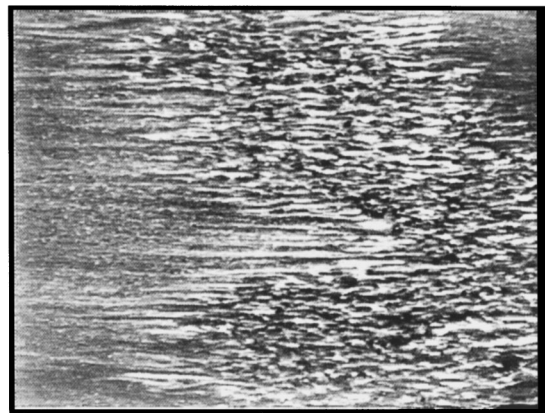

FIG. 1. Shown in the above photograph is the intermittent turbulent state in plane Couette flow (PCF) at a Reynolds number of 500. In this side view the walls are moving horizontally and the average velocity gradient is normal to the plane of this photograph. This side view is illuminated with white light and the flow is seeded with reflecting Iriodin particles so that the laminar regions appear featureless while the turbulent spots have light reflectance variations. The photograph shows a region in the center portion of the working region in the (x,y) plane $\sim 10h$ from the top and bottom edges of the belt and $\sim 140h$ from the streamwise edges of the working region.
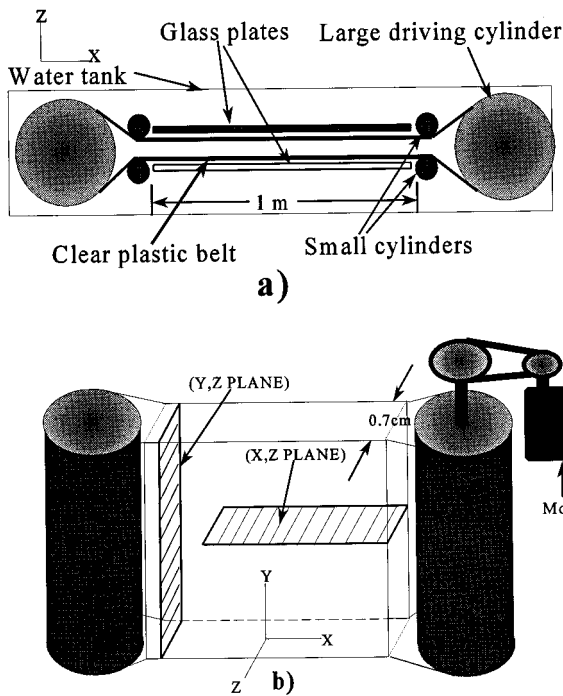
FIG. 2. (a) A schematic drawing of the plane Couette flow apparatus in a horizontal plane [the (x,z) plane]. Two large cylinders, two pairs of small cylinders, two glass plates, and a clear plastic belt are arranged in a water tank as shown. (b) A schematic drawing that illustrates the flow channel and the plane Couette flow geometry in 3D. The streamwise x and cross-stream z directions are in the horizontal plane while the spanwise y direction is vertical. Laser light sheet visualizations are done in the (x,z) plane and the (y,z) plane as shown.

bulent spots. This design simplification is made possible because the two walls are part of the same endless transparent film belt (363.0 cm long, 25.4 cm wide, and 0.16 mm thick). We use a transparent belt so flow visualization may be used. As shown schematically in Fig. 2, two pairs of small rotating Plexiglass cylinders and two large rotating Plexiglass cylinders guide the endless belt into the parallel wall configuration. The endless belt is driven by one of the two large cylinders placed at opposite ends of the system. The belt-driving cylinder is mechanically coupled to an external motor through a 100:1 planetary gearbox. This speed reduction allows us to operate at a Reynolds number between 100 and 700 while maintaining sufficient power to drive the system with a high resolution in the speed. The gap between the two parallel walls is controlled by adjusting the two pairs of smaller cylinders. In this experiment, the gap is 7.00 mm. The two pairs of small cylinders are also used to adjust the tension in the belt by moving them closer together or farther apart, while the axes of the two large cylinders remain fixed. To stabilize the belt against vibrations, to help in visualization, and to define a test section of 1 m, two glass plates (one black and the other transparent) are placed parallel to the film belt. These glass plates, which have a longer spanwise length than the belt, also provide consistent open end conditions at the top and bottom edges of the belt. In the remainder of this paper, x is in the streamwise direction, y is in the spanwise direction, and z is in the cross-stream direction as shown in Fig. 2. Using h as a length scale, the transverse aspect ratio

Γ_y (dimensionless width of the channel) is $\Gamma_y = 72.7$. The longitudinal aspect ratio Γ_x (dimensionless length of the channel) is $\Gamma_x \approx 340$ (since the length of the straight section of the channel is changed when the belt tension is changed this is an approximate value). Near the two ends of the system where fluid particles enter the channel, the velocity field will require some length along the x direction (or equivalently some time) before a linear profile is established. Assuming a Blasius boundary layer growth of the flow profile by the wall, we estimate that 90% of the flow channel and all of the test section are fully developed linear Couette flow at $R = 500$. We have also verified by direct measurement that the profile is linear as high as $R = 300$ [2,16]. The entire system is contained in a glass tank filled with water of $v \approx 0.01$ S (stoke, S, is a unit of kinematic viscosity).

We visualize the flow by mixing the water with a small amount of Merck Iriodin 100 Silver Pearl ($\leq 0.02\%$ by volume). These thin and flat reflective mica platelets, of diameter ≈ 10 μm, align on average with the stream planes of the flow (these are the planes tangent to the 3D velocity field, known as streamlines in a 2D velocity field). Similar platelet-type agents, such as Kalliroscope or aluminum powder, have previously been used to visualize vortex structures and turbulent spots [17–20]. The platelets respond almost instantaneously to local changes in the flow pattern giving a change in the light reflectance pattern whenever a change in the velocity pattern occurs [20]. This visualization method also makes an excellent indicator of turbulence on small scales [21]. The turbulent regions are indicated by a rapid fluctuation in the reflected light intensity field, whereas the laminar region's light reflectance is steady. The evolution of the visualized flow pattern is recorded using a video camera and subsequently digitized and analyzed by image processing. We have also visualized 2D projections of the velocity *field* in both the vertical and horizontal cross sections [see Fig. 2(b)]. This was done by seeding the flow with a white ceramic powder (Pyroceram 7575, 100 Mesh) and illuminating the flow with an argon laser light sheet. Both the (x,z) and (y,z) planes were illuminated by changing the orientation of the light sheet. Light scattered by the particles in the light sheet is reflected in both orientations by a mirror into a camera for recording.

Externally applied perturbations that trigger turbulent spots are made by injecting turbulent jets into the laminar flow. Previous experiments that studied the onset used a well-controlled jet in the z direction from a 2-mm hole in the dark glass plate. This method requires that a small hole be placed in the belt so that the flow from the jet may pass into the channel. To avoid disturbances from this hole we have injected perturbations from the side in the spanwise or y direction from a syringe needle placed near the side of the channel. Once a turbulent spot is initiated, its evolution is visualized by shining light through the transparent belt and observing the light reflected from the Iriodin in the flow as described above. Our system allows for most of the flow across and along the belt [the (x,y) plane] to be visualized.

III. RESULTS

A critical Reynolds number R_c, where finite-amplitude perturbations produce persistent turbulent spots, has been

measured to be as low as 325 in this system [12]. Turbulent spots were initiated by the perturbation method described above at given values of R above R_c. Their subsequent evolution was recorded in the (x,y) plane. In this zero mean flow apparatus, the spots remain stationary over the time scale of the rapid fluctuations within the turbulent regions. This is consistent with the behavior seen in other systems where turbulent spots travel with the mean flow [18–20,22]. In the laboratory frame of reference, however, we have also observed a slow spatial and temporal evolution of the turbulent regions. This evolution is much slower than light reflectance fluctuations within the turbulence. Above R_c, turbulent spots may form a variety of temporary shapes. Shapes can be distinguished because of a rough laminar-turbulent interface or edge, as can be seen in Figs. 1 and 3(a). These shapes include forms that are similar to the spots observed in plane Poiseuille flow [18] and in the Blasius boundary layer [17]. As these various turbulent patches evolve they grow, split, shrink, and merge. The turbulent regions have never been observed to settle into a regular pattern as is seen in spiral turbulence in Couette-Taylor flow [19,20,22]. The turbulent patches generally do not have straight spanwise edges. The edges of the turbulent patches are either curved or straight with the straight edges inclined to the horizontal [see Figs. 1 and 3(a)].

At an R greater than R_c (which depends on the amplitude of the perturbation and perturbation type [12,2]) the intermittent turbulence will last as long as is experimentally feasible. The fraction of the total space that is turbulent increases as R is increased. At higher R, the turbulent regions connect to form a network. At $R=600$ all of the space in the test section quickly becomes turbulent after the spanwise perturbation is applied to the flow.

As mentioned above, we have observed that the position and shape of the turbulent spots evolve much more slowly than the time for light reflectance fluctuations within the turbulent regions. Figure 3 illustrates these small-scale light reflectance fluctuations within a typical turbulent region at $R=420$. Figure 3(a) shows an image of a typical turbulent region that changes shape slowly compared with the light reflectance fluctuations. Figure 3(b) illustrates the rapid fluctuation of Fig. 3(a). The intensity of each pixel in Fig. 3(b) is proportional to the root-mean-square intensity fluctuation over 0.2 s of a corresponding pixel in Fig. 3(a). Dark areas do not fluctuate whereas pixels with increasing brightness have increasing fluctuations.

Figure 3(a) which shows one video frame of the turbulent region, also illustrates a typical feature of the visualized flow: we always observe that the turbulent regions exhibit finite-length streamwise streaks. In fact, both Figs. 3(a) and 3(b) exhibit this streakiness. Figure 3(b) shows that the streaky structures are quickly evolving.

The streamwise streaks of the image in Fig. 3(a) can be seen more clearly in the Fourier-transformed image of Fig. 3(a) shown in Fig. 4. Figure 4 illustrates this anisotropic feature of Fig. 3(a) in that an oval wave-number spectrum lies along the spanwise direction to a greater extent than the streamwise direction. The peak at $K_y \approx 5$ corresponds to the horizontal pixel lines in the video image. It appears that the features in the image have most of their Fourier components in only one direction.
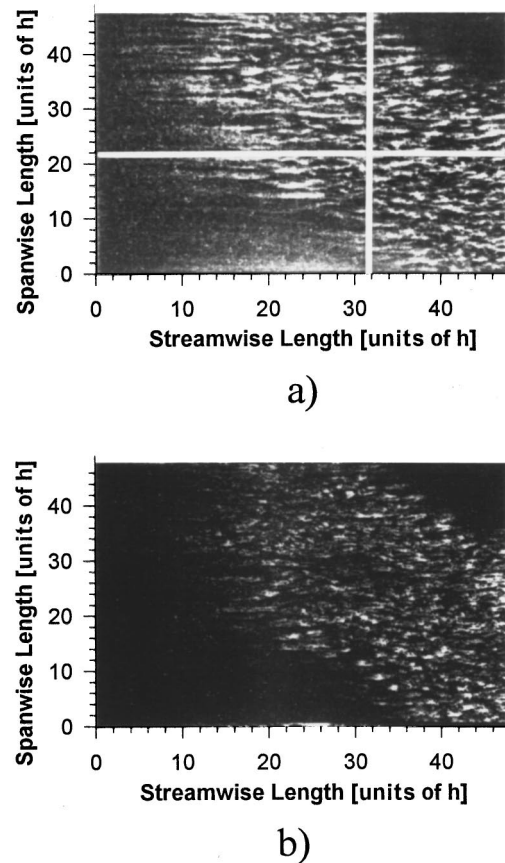

a)

b)

FIG. 3. (a) This image shows the light reflectance field from a typical turbulent spot in the test region of the PCF channel at $R=420$ using Iriodin particles. The photograph shows a region in the center portion of the working region in the (x,y) plane $\sim 10h$ from the top and bottom edges of the belt and $\sim 140h$ from the streamwise edges of the working region. The streamwise streaks in the image are a typical feature of the spots of all shapes. The straight lines drawn through the image show where the space-time data in Figs. 5 and 6 were obtained. (b) This image illustrates how the turbulent region in (a) is fluctuating in light intensity. Five consecutive images are recorded over 0.2 sec. At a given position in the image the standard deviation σ is calculated from the five images. The resulting image of $\sigma(x,y)$ is plotted on a gray scale and is shown in (b) Black shows a zero σ or no light fluctuation over 0.2 sec. Brighter areas show increasing fluctuations. The small bright dots in the otherwise dark laminar regions are caused by random reflections from the Iriodin visualization particles.

The broadband spectrum from a singe image is difficult to interpret, especially with the rapid temporal evolution of the smaller scale features in the visualization. We therefore took 1D pixel slices along the x and y directions, as shown in Fig. 3(a) and calculated the time-averaged autocorrelation. Figures 5(a) and 6(a) show the time evolution of the slices, i.e., the space-time diagrams along the x and y directions, respectively. Figures 5(b) and 6(b) show the time-averaged autocorrelation functions calculated from the turbulent regions in the data in Figs. 5(a) and 6(a). These data show primary autocorrelation minima. The valleys are the characteristic distances L_x and L_y between a bright and dark (or vice versa) area in the turbulence. Consistent with the streakiness of the visualization, L_x is larger than L_y. In addition, a spatially
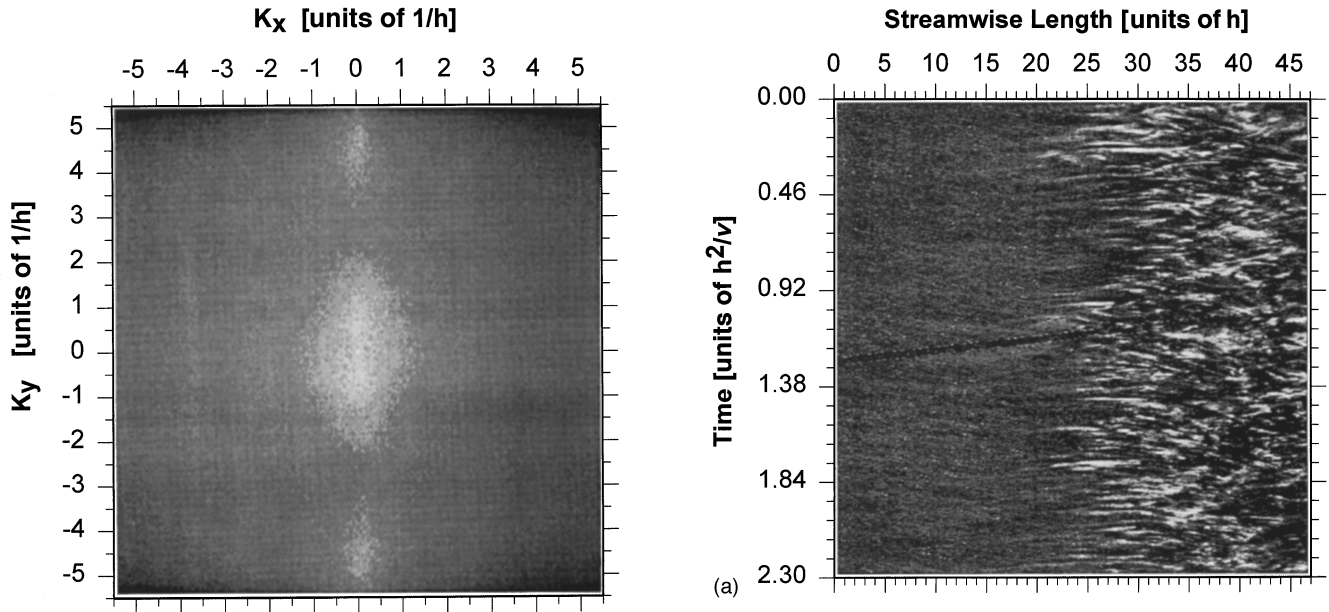
K$_X$ [units of 1/h]

FIG. 4. Shown above is the 2D Fourier transform of the image shown in Fig. 3(a). The anisotropic light intensity distribution is seen by the oval shaped 2D Fourier transform. Streaky structures in the visualization using Iriodin particles have larger Fourier components in the spanwise direction than the streamwise direction. The high K_y peak corresponds to the horizontal pixel lines of the video image.

averaged temporal autocorrelation function, derived from the data in Fig. 6(a) is shown in Fig. 6(c). This shows the characteristic time T for a bright area to become dark (or vice versa). This time characterizes the fluctuation time within the turbulent spots in the visualization.

We have seen autocorrelation minima that are similar to those described above for typical spots in a wide range of R. Within an R range of $380 \leq R \leq 650$, we found that $0.74 \leq L_x \leq 3.6$, $0.94 \leq L_y \leq 1.67$, and $0.07 \leq T \leq 0.13$. L_x and L_y are scaled by h and T is scaled by h^2/v, as shown in Figs. 5 and 6. L_x, L_y, and T depend on the space-time region within a turbulent spot where the measurement is made. Measurements of L_x, L_y, and T increase when made near the edge of a spot and decrease when made near the center. This is caused by the strong streaks that appear near the edges of the spots. Measurements of L_x, L_y, and T are independent of position in the turbulence when the test region becomes fully turbulent.

IV. STRUCTURES

Light sheet visualization within the gap has also been done in the plane Couette flow apparatus as described above. Figures 7 and 8 show time-exposure photos (or streak photos) of the gap in the (x,z) and (y,z) planes. In addition, we have videotaped the particle motion in the laser light sheets at $R=440$. The time exposure of our charge-coupled-device (CCD) camera and the velocity of the walls were such that the wall travels ≈ 0.5 cm during one exposure, i.e., a particle travel $\sim h$ at the wall in one frame. In fact, we are not able to distinguish individual particles at the wall in the video visualizations of the (x,z) plane. In the center region of the chan-
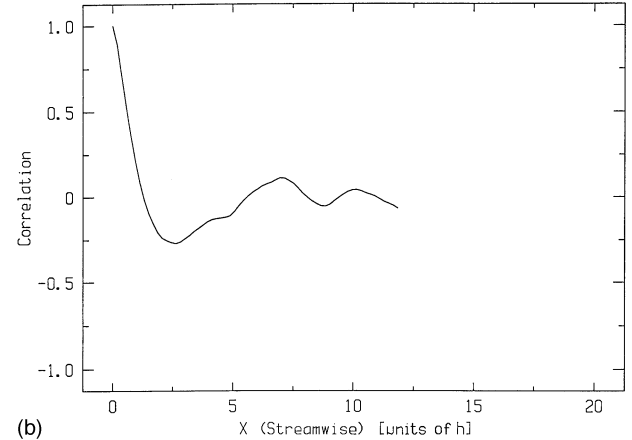
Streamwise Length [units of h]

FIG. 5. Time evolution of a 1D (512) pixel line along the x direction is shown in (a). The position of this 1D line in relation to the (x,y) plane in the visualization using Iriodin particles is shown in Fig. 3(a). The typical spatial-temporal evolution in the streamwise direction does not show any apparent features. From these spatial and temporal data (space-time diagram) we have calculated the spatial autocorrelation for each spatial line in the turbulent region. The time-averaged autocorrelation, shown in (b), shows a characteristic valley in negative correlation. This minimum is the characteristic distance L_x between a bright and a dark (or vice versa) region in the turbulence.

nel we can see particle streaks in each frame that indicate particle motion during the exposure. In the laminar regime we are only able to distinguish a region of $\sim h$ about the center zero velocity line in the (x,z) plane. The particles near the wall in the (y,z) plane spend $\sim 1/10$ of the CCD camera exposure time in the light sheet so that the laminar flow appears as flickering points of light. In the turbulent regime, we are clearly able to distinguish the particle streaks in most of the channel, except very close to the walls in both light sheet orientations. The laminar and turbulent regimes are clearly distinguishable in the video visualizations.

Figure 7(a) shows a feature often seen in the (x,z) plane: motion in the z direction within a turbulent spot.
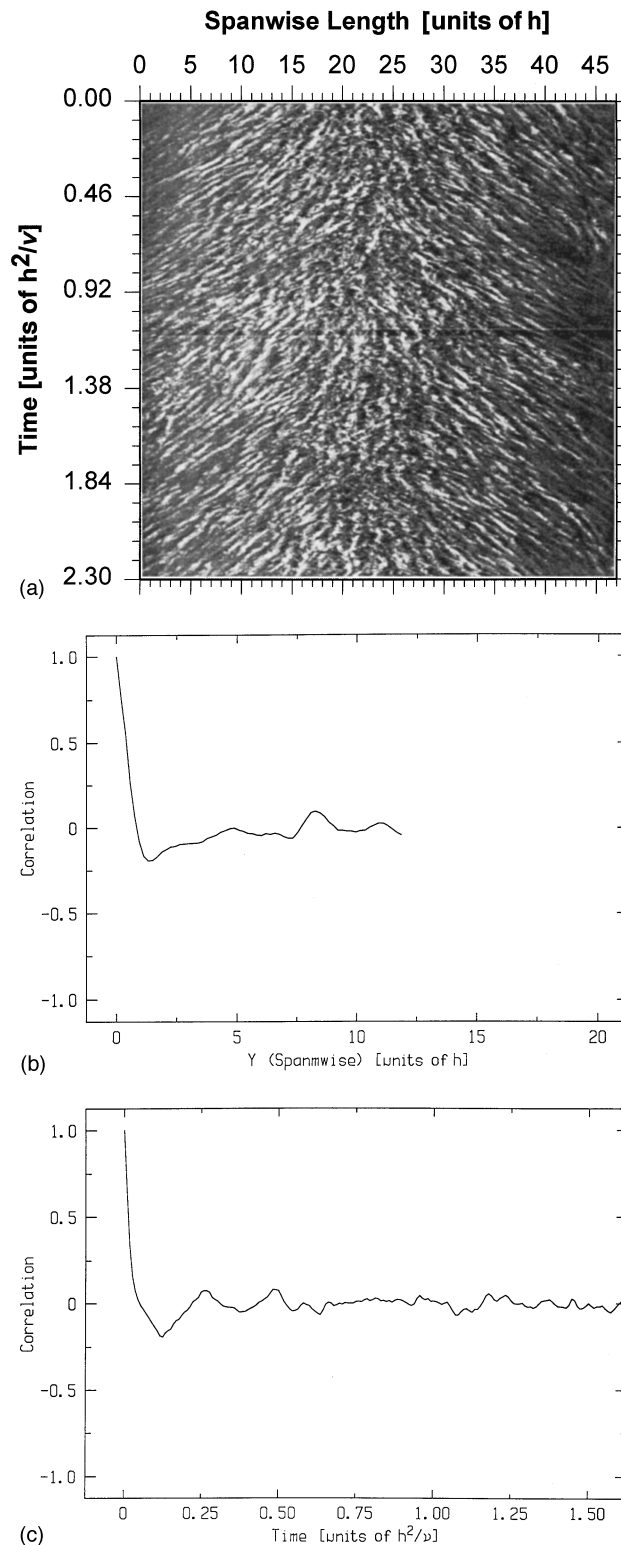
FIG. 6. Time evolution of a 1D (512) pixel line along the y direction is shown in (a). The position of this 1D line in relation to the (x,y) plane in the visualization using Iriodin particles is shown in Fig. 3(a). Previously reported traveling waves that propagate outward from the spot in the spanwise direction are shown in (a). From this spatial and temporal data (space-time diagram), we have calculated the spatial autocorrelation for each spatial line in the turbulent region. The time-averaged autocorrelation shown in (b) shows a characteristic valley in negative correlation. This minimum is the characteristic distance L_y between a bright and a dark (or vice versa) region in the figure. A comparison with Fig. 5 shows that L_x is larger than L_y, which is consistent with the finite length and width of the streaks in the turbulence. (c) shows a spatially averaged temporal autocorrelation function derived from the data in (a). The valley in negative correlation shows the characteristic time T for a bright area to become dark (or vice versa). T is the characteristic time for fluctuations within the turbulence in the image.
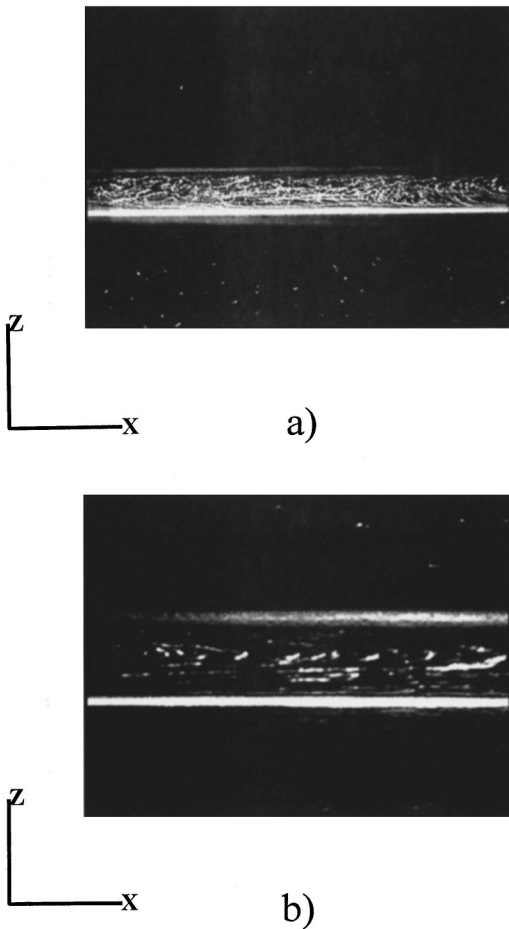
Z
X
a)

Z
X
b)

Y
Z
a)

Y
Z
b)

FIG. 7. Figure 7 shows time exposure photographs or streak photographs of Pyroceram particles seeded in the flow at $R=380$. The particles in this photograph are illuminated with a light sheet within the gap in the (x,z) plane. The parallel lines are light reflections from the transparent belt and indicate the belt edge. Photograph (a) shows velocity components in the z direction within the turbulent spot, as we have repeatedly observed. The curved particle trajectories just outside the spot can also be seen on the far right of this photo. Photograph (b) shows another view in a different case of the cross-channel flow just outside a turbulent spot. These strongly curved particle trajectories are outside a turbulent spot that is to the right, outside the field of view. The beginning of the distorted velocity profile in the (x,z) plane is shown in photograph (b).

The behavior inside a spot is complex with no distinguishable structures in the instantaneous (x,z) plane. We have also observed cross-channel flow just outside the turbulent spot. In fact, the particle trajectories, shown in Fig. 7, are strongly curved just outside the spot. The video visualizations in the (x,z) plane clearly show that fluid particles traveling toward the spot by one wall may travel across the channel and move away from the spot along the other wall. No such cross-channel motion is seen in the laminar flow. The velocity profile in the x direction $V_x(z)$ has been observed to change considerably just outside the turbulent region. We have seen several cases where the $V_x(z)$ zero velocity line moves toward one of the walls. Just outside the turbulence the particles reverse directions along highly curved particle trajectories. The particles near the $V_x(z)$ zero line gain speed in the z direction. Turbulence has repeatedly appeared near
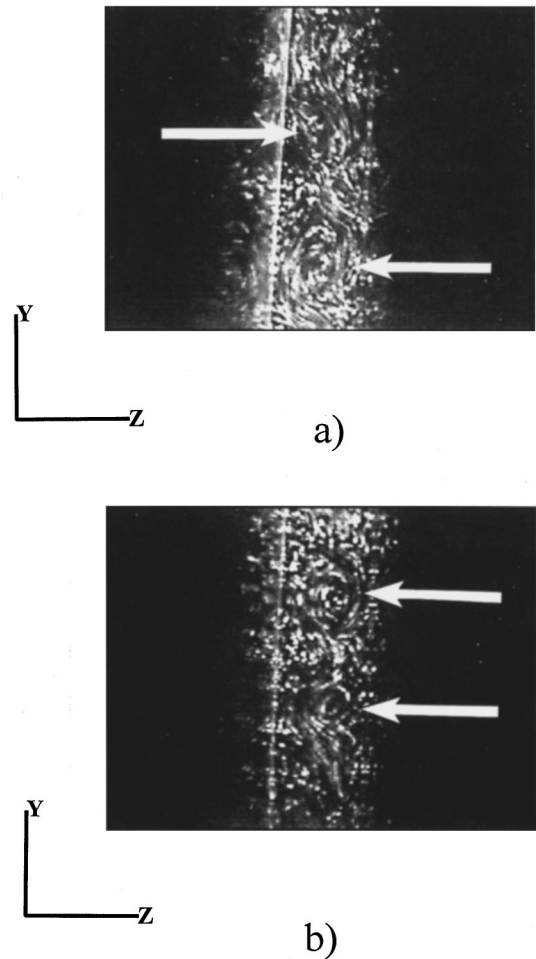
FIG. 8. Streak photographs of the gap in the (y,z) plane using Pyroceram particles are shown. These photographs show the cross section of vortical structures in the (y,z) plane at $R=380$ as indicated by the arrows. The parallel lines (brighter line on the left side) are light reflections from the transparent belt and indicate the belt edge. Outside these lines some reflections from the wall are also present (these reflections also indicate the belt edge). This is a cross section of the streamwise vortices that we have observed to pervade these spots. The presence of these structures correlates well with the streaks in the (x,y) plane visualizations using Iriodin particles and shows that the streaks are streamwise vortices. Photograph (a) shows disordered flow between vortices. Photograph (b) shows the quiescent flow between vortices.

these curved trajectories. Figure 7 shows several different cases of this behavior. We have not seen any oscillatory behavior in the distorted laminar profile near a turbulent spot in the (x,z) plane.

Although we have not distinguished any instantaneous flow structures in the (x,z) plane with light sheet visualization, we have observed vortical structures in the (y,z) plane as shown in Fig. 8. The circular structures in the figure are cross sections of streamwise vortices that we have observed to pervade these spots. Their temporal behavior is quite complex and includes events such as vortex creation, vortex destruction, and vortex motion. The vortices seem to form and disappear quickly, possibly because the structures move in the streamwise direction out of the light sheet. Particles can also be seen to enter and leave the light sheet, indicating an

x component to the flow. The regions between vortices may be quiescent or have a disordered flow in the (y,z) plane (see Fig. 8). In the interior of a turbulent spot there is no preference for vortices of positive or negative vorticity, nor is there any systematic pattern to the vortex behavior. At the interface between laminar and turbulent flow, however, an average motion of these vortex structures away from the turbulent region occurs. Before the turbulence arrives, we have observed a shear flow with strong components in the (y,z) plane. In the (y,z) plane the particles appear to travel in one direction near one wall and in the opposite direction near the opposite wall. This shear flow next forms several large vortices all of the same vorticity as the background shear flow, i.e., the shear flow appears to roll up into streamwise vortices. These vortices almost fill the entire gap and they move away from the spot. Vortices of opposite vorticity next form between these large vortices and the complex flow described above occurs. The vortices in the interior of the spots have a smaller average diameter ($\sim h$) and a larger average angular velocity ($\sim 4\pi$ rad/sec) than the vortices at the edge of the spot ($\sim 2\pi$ rad/sec).

The presence of the streamwise vortex structures correlates well with the streakiness in the (x,y) plane visualizations and show that the streaks are streamwise vortices. Other vortex structures, such as Taylor vortices, also show this banded or streaklike appearance in similar visualizations. The streamwise vortices observed by Dauchot and Daviaud [13] in the modified PCF also manifested this streakiness. We note that the streaks or streamwise vortices tend to be stronger at the edge of the spot, while the vortices inside of a spot are more likely to be inclined to the streamwise direction.

V. DISCUSSION

The identification of the streaks in the (x,y) plane visualization as streamwise vortices makes possible a more physical interpretation of the autocorrelation lengths L_x and L_y and the autocorrelation time T. L_x is the typical length of the streamwise vortices in the x direction. L_y is the typical width of these structures along y. T is the typical time it takes a vortex to grow at a given position, to decay at a given position, to move half its width, or to move and change simultaneously. We have verified in the (y,z) plane light sheet visualizations that T is a typical fluctuation time and L_y is a typical spanwise length of the streamwise vortices.

The curved particle trajectories just outside the turbulent spot, as shown in Fig. 7, indicate the presence of instantaneously curved streamlines in the (x,z) plane. There are several well-known cases where shear flows with curved streamlines become centrifugally unstable. In the Taylor, Gortler, or Dean centrifugal instabilities, for example, the curved streamlines lead to Taylor vortices, Gortler vortices, or Dean vortices. Each of these resultant vortex structures have their axes in the direction of the background flow and would be considered streamwise in their respective geometries. We have also observed that the strongest streamwise vortices tend to appear toward the edge of the turbulence. This suggests that a centrifugal instability may be generating the streamwise vortices at the edges of the spots. The (y,z) plane visualization, however, shows that the interface region

also has flow components in the y direction. The flow components in the y direction are slower than the flow components in the x direction. This slower flow exhibits the periodic behavior often associated with an instability of an inflectional velocity profile that generates vorticity near the inflection point. This suggests another possible instability mechanism where the streamwise vortices are generated by an Orr-Sommerfeld-type instability of an unstable profile in the (y,z) plane. Since our visualizations are *projections* of the true flow near the interface, we cannot determine which instability, if either, is the true mechanism. A 3D particle image velocimetry measurement is needed to learn what mechanism generates the vortices at the spot's edge. Although we have not been able to determine the vorticity generating mechanism in this study, it is also possible that another mechanism more specific to the conditions at the spot interface generates the streamwise vortices at the edge. In the following we present such an alternative mechanism where the processes of vortex stretching and vortex tilting explain the flow we observed outside of the turbulence [i.e., cross-channel flow outside the turbulence observed in the (x,z) plane (see Fig. 7) and the shear flow and roll up outside the turbulence seen in the (y,z) plane].

The constant background vorticity $\mathbf{w}$ of the plane Couette flow is in the spanwise direction, i.e., $\mathbf{w}=(0,w_y,0)$. This is just the vorticity of the linear velocity profile (vorticity is a measure of the local rotation or spin of a fluid particle and is given by $\mathbf{w}=\nabla\times\mathbf{V}$). Just as $\mathbf{V}$ is often described using streamlines, the vorticity field $\mathbf{w}$ uses the construct of vortex lines, i.e., lines to which $\mathbf{w}$ is tangent, to describe $\mathbf{w}$. These vortex lines follow the same fluid particles or material lines in the absence of viscosity. When there is a turbulent spot in the proximity of this background flow the evolution of a vortex line is given by [23] $Dw_y/Dt=w_y(\partial V_y/\partial y)$ and $Dw_x/Dt=w_y(\partial V_x/\partial y)$, where D/Dt is the convective derivative [23] and we have neglected viscosity. The first equation describes vortex stretching; e.g., a vortex line in the y direction increases in vorticity when subjected to a positive ($\partial V_y/\partial y$) gradient [see Fig. 9(a)]. This equation also expresses the physical fact that a fluid particle, when extended in the y direction by $\partial V_y/\partial y$, must spin faster or increase w_y in order to conserve angular momentum. The second equation describes vortex tilting where w_y, when subjected to a perpendicular velocity gradient $\partial V_x/\partial y$, will rotate or tilt the vortex line to give it an x component w_x. A vortex line w_y that follows a material line along y will be tilted by $\partial V_x/\partial y$ because the larger velocities will move the material line more than the smaller velocities. If a turbulent spot is generating in the laminar flow a streamwise velocity that changes with respect to the spanwise direction [i.e., $\partial V_x/\partial y$ as shown in Fig. 9(a)], then the background vorticity lines in the laminar flow w_y could be tilted to generate streamwise vorticity w_x. In fact, the shear flow in the (y,z) plane observed outside the turbulence and described above corresponds to this w_x. The w_y background vorticity could also be stretched if a turbulent spot is, for example, generating a spanwise flow that is increasing in the spanwise direction [i.e., a positive $\partial V_y/\partial y$, as shown in Fig. 9(a)]. Alternatively, once a vortex line has been tilted toward the x direction to produce w_x, a $\partial V_x/\partial x$ gradient will stretch this streamwise vortex line. The increase in vorticity from the vortex stretching is manifested
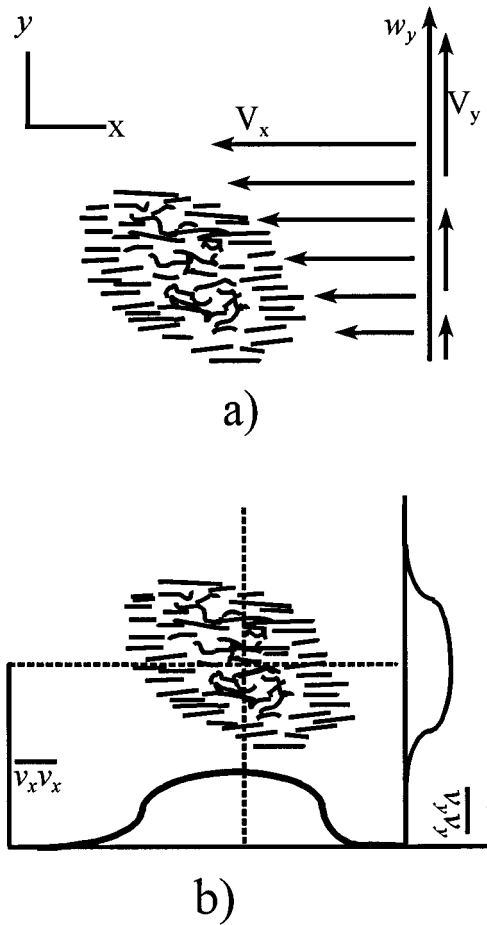
FIG. 9. (a) Illustrates the vortex stretching and vortex tilting that could occur outside of a turbulent spot. The vortex line in the laminar flow w_y, when subjected to a perpendicular velocity V_x that changes in the y direction, as shown, will rotate or tilt the vortex line counterclockwise to give it an x component w_x. The same vortex line w_y increases in vorticity when subjected to a velocity gradient where V_y increases in the y direction as shown. The separation of the flow into laminar regions and turbulent regions necessarily implies a gradient in Reynolds stress at the spot interface as shown schematically in (b). The two parts of the turbulence energy $\overline{v_x v_x}$ and $\overline{v_y v_y}$ along the dotted lines are shown. The change in Reynolds stress at the interface also induces a pressure gradient in the laminar flow that stretches and tilts the laminar vortex lines into turbulent streamwise vortices.

as vortices of $\sim 2h$ diameter because of the geometric constraint of the channel. The exact process is unclear from the visualization evidence. The cross-channel flow seen outside the spot in the (x,z) plane, shown in Fig. 7(a) suggests that w_y may be first stretched into $\sim 2h$ diameter vortices along y and then tilted into streamwise vortices. The shear flow and roll up outside the turbulence seen in the (y,z) plane, described above, suggests that w_y may first be tilted into streamwise vorticity w_x and then stretched into streamwise vortices. Because both visualization planes indicate vortex tilting and stretching, the vortex stretching and vortex tilting probably occur simultaneously. The final result is that the background w_y is stretched and tilted into streamwise vortices at the spot's edge. This idea could easily be tested and the details further examined by measuring the velocity field

outside a spot in plane Couette flow.

Further inside the spot, the vortices' average diameter decreases while the average angular velocity of a vortex increases. Considerable cross-channel flow is also seen [see Fig. 7(a)]. This suggests that vortex stretching and tilting are also occurring between the center of the spot and the streamwise vortices at the edge. In order for vortices to be stretched and tilted in the interior of the spot there must be velocity gradients present. The velocity gradients present at a given vortex are probably the result of the complex interactions it has with other vortices. This complex behavior observed in the (y,z) plane was described above. The effect of this complex behavior in the turbulence on the laminar flow may be analyzed by using the standard Reynolds decomposition of the velocity $\mathbf{V}^*$ and the pressure P^* into an average and a fluctuating part [23] (i.e., $\mathbf{V}^*=\mathbf{V}+\mathbf{v}$ and $P^*=P+p$, where $\mathbf{V}$ and P are the average velocity and average pressure; $\mathbf{v}$ and p are the fluctuating velocity and fluctuating pressure). This decomposition is substituted into the Navier-Stokes equations and the continuity equation. When an ensemble average is taken over identically prepared turbulent spots, the resulting equations are

$$V_x \frac{\partial V_x}{\partial x} + V_y \frac{\partial V_x}{\partial y} = -\frac{1}{\rho}\frac{\partial P}{\partial x} - \frac{\partial \overline{v_x v_x}}{\partial x} - \frac{\partial \overline{v_x v_y}}{\partial y} - \frac{\partial \overline{v_x v_z}}{\partial z},$$

$$V_x \frac{\partial V_y}{\partial x} + V_y \frac{\partial V_y}{\partial y} = -\frac{1}{\rho}\frac{\partial P}{\partial y} - \frac{\partial \overline{v_y v_x}}{\partial x} - \frac{\partial \overline{v_y v_y}}{\partial y} - \frac{\partial \overline{v_y v_z}}{\partial z},$$

where the viscosity, the explicit time dependence of $\mathbf{V}$, and V_z are assumed to be smaller effects. The fluctuation correlations such as $\overline{v_x v_y}$ that result from the nonlinearity are called the Reynolds stress, and their spatial derivatives act as a forcing on the mean flow. Because the flow is separated into laminar and turbulent regions, the Reynolds stress is appreciable in a turbulent region and negligible in a laminar region. The separation of the flow into laminar and turbulent regions necessarily implies a gradient in Reynolds stress near a spot interface as shown schematically in Fig. 9(b). The lack of fluctuation in the laminar flow also means that the average velocity and average pressure are approximately equal to the actual velocity and actual pressure in a laminar region. The visualizations, however, indicate considerable distortion of the velocity profile outside a turbulent region where fluctuations are negligible. This suggests that the change in Reynolds stress at an interface is inducing a pressure gradient in the laminar flow. The terms $-(1/\rho)(\partial P/\partial x)$ and $-(1/\rho)(\partial P/\partial y)$ accelerate the laminar flow outside the spot. This acceleration is shown on the left-hand side of the equations above and includes factors such as $\partial V_x/\partial y$ that could tilt w_y, $\partial V_x/\partial x$ that could stretch w_x, and the gradient $\partial V_y/\partial y$ that could stretch w_y. It is therefore possible that the spatial gradient in Reynolds stress generated by a turbulent spot induces a pressure gradient in the laminar flow that causes the vortex stretching and tilting in the laminar flow. This vortex stretching and tilting generates streamwise vortices at the edge of a turbulent spot. They are further tilted and stretched through complex vortex interactions to generate the spatially changing Reynolds stress. The absence of a straight spanwise interface shows that the vorticity generating mechanism at the interface is enhanced when the interface is inclined. This

further suggests that vortex stretching and tilting is the cause of the streamwise vortices because a spatial distribution of Reynolds stress in this shape is likely to create pressure gradients in both the x and y directions (i.e., induce both $-(1/\rho)(\partial P/\partial x)$ and $-(1/\rho)(\partial P/\partial y)$ pressure gradients in the laminar flow) that are very likely to generate vortex tilting and vortex stretching velocity gradients. Because the changing Reynolds stress due to the fluctuations in the spot leads to the vortex stretching and tilting, the subcritical nature of the intermittent state may be explained. A perturbation will lead to a self-sustaining turbulent spot if it is large enough to generate enough Reynolds stress to modify the nearby laminar flow so that there is vortex tilting and stretching.

Figure 6(a) shows the traveling waves, previously reported in Ref. [2], that propagate outward from the turbulent region. Similar phenomena in spiral turbulence in Couette-Taylor flow have been previously reported [20,22]. Tillmark and Alfredsson [11] have also reported seeing traveling waves with the wave crests aligned in the streamwise direction that move in the spanwise direction. The streamwise extent of the waves that they observed was quite large (~ 10 h) compared to the waves we observed (~ 3 h). They also reported that the waves were overtaken by the spreading of the turbulent region, while the waves we have observed were sustained as long as the turbulence was present. In the full visualization of the (x,y) plane these waves are manifested as the horizontal streaks or streamwise vortices traveling in the spanwise direction away from the turbulence. We have also directly observed these traveling vortices in the (y,z) light sheet. The vortex stretching and tilting interpretation given in the discussion above suggests that these traveling waves result from the vortex stretching and tilting that occurs

at the interface. An inclined laminar-turbulent interface has the property that the vortices at the edge can travel away from the turbulence into laminar flow. The stable spiral turbulence pattern in Couette-Taylor flow also has an interface that is inclined to the background shear flow. The up and down moving waves within the turbulence may help to explain the end effects observed in spiral turbulence [20,22].

VI. CONCLUSION

We have observed in a PCF apparatus streamwise vortex structures in turbulent spots. Characteristic lengths, widths, and fluctuation times have been measured. The streamwise vortices have been directly visualized in the spanwise cross-stream (y,z) plane verifying these measurements. At lower R, the streamwise vortices are more pronounced near the edges of the spots. These edge vortices also travel away from the turbulent spots forming traveling waves. The vortices at the edge become tilted and stretched inside the turbulent spot. The turbulent fluctuations within a turbulent spot generate a stress in the laminar flow that may cause the vorticity in the laminar flow to be stretched and tilted into streamwise vortices.

[1] V. Romanov, Funkt. Anal. Appl. **7**, 137 (1973).

[2] F. Daviaud, J. Hegseth, and P. Bergé, Phys. Rev. Lett. **69**, 2511 (1992).

[3] Y. Pomeau, Physica D **23**, 1 (1986); **51**, 546 (1991).

[4] S. A. Orszag and L. Kells, J. Fluid Mech. **96**, 159 (1980).

[5] A. Lundbladh and A. Johansson, J. Fluid Mech. **229**, 499 (1991).

[6] M. Nagata, J. Fluid Mech. **217**, 519 (1990).

[7] J. Lerner and E. Knobloch, J. Fluid Mech **189**, 117 (1988).

[8] B. Dubrulle and J. P. Zahn, J. Fluid Mech. **231**, 561 (1991).

[9] H. Reichardt, Z. Angew, Math. Mech. **26**, 1 (1956).

[10] H. J. Leutheusser and V. H. Chu, J. Hydr. Div. ASCE **97**, 1269 (1971).

[11] N. Tillmark, and P. H. Alfredsson, J. Fluid Mech. **235**, 89 (1992).

[12] O. Dauchot and F. Daviaud, Europhys. Lett. **28**, 225 (1994).

[13] O. Dauchot and F. Daviaud, Phys. Fluids **7**, 901 (1995).

[14] J. M. Robertson and H. F. Johnson, J. Eng. Mech. Div. ASCE, **96**, 1171 (1970).

[15] M. Aydin and J. Leutheusser, Rev. Sci. Instrum. **50**, 1362 (1979).

[16] J. Hegseth, F. Daviaud, and P. Bergé, in *Proceedings of the Conference on Ordered and Turbulent Pattern in Taylor-Couette Flow, Columbus, Ohio, 1991*, edited by C. D. Andereck (Plenum, New York, 1991).

[17] B. J. Cantwell, D. Coles, and P. Dimotakis, J. Fluid Mech. **87**, 641 (1978). Also see M. Gad-El-Hak, R. F. Blackwelder, and J. J. Riley, *ibid*. **110**, 73 (1981).

[18] D. R. Carlson, S. E. Widnall, and M. F. Peeters, J. Fluid Mech. **121**, 487 (1983).

[19] D. Coles, J. Fluid Mech. **21**, 385 (1965). Also see C. W. Van Atta, *ibid*. **25**, 495 (1966).

[20] J. Hegseth, Ph.D. dissertation, Ohio State University, 1990 (unpublished).

[21] K. W. Schwarz, Phys. Rev. Lett. **64**, 415 (1990).

[22] J. J. Hegseth, C. D. Andereck, F. Hayot, and Y. Pomeau, Phys. Rev. Lett. **62**, 257 (1989).

[23] D. J. Tritton, *Physical Fluid Dynamics* (Oxford University Press, New York, 1988).